INL/MIS-21-64890-Revision-0

Comparison between Point Reactor Kinetics and Spatial Dynamics for the NRAD Reactor

October 2016

Javier Ortensi, Benjamin A Baker, Andrew Hummel

Changing the World's Energy Future

INL is a U.S. Department of Energy National Laboratory operated by Battelle Energy Alliance, LLC

INL/MIS-21-64890-Revision-0

Comparison between Point Reactor Kinetics and Spatial Dynamics for the NRAD Reactor

Javier Ortensi, Benjamin A Baker, Andrew Hummel

October 2016

Idaho National Laboratory
Idaho Falls, Idaho 83415

http://www.inl.gov

Prepared for the
U.S. Department of Energy
Under DOE Idaho Operations Office
Contract DE-AC07-05ID14517, DE-AC07-05ID14517

INTEROFFICE MEMORANDUM

Idaho National Laboratory INL

Date: November 22, 2016

To: Rick Gunderson

cc Andrew Smolinski, Gilles J. Youinou

From: Javier Ortensi, Benjamin Baker, Andrew Hummel

Subject: Comparison between Point Reactor Kinetics and Spatial Dynamics for the NRAD Reactor

The purpose of this memorandum is to provide insights into the expected differences between Point Reactor Kinetics (PRK) and spatial dynamics (SD) simulations of the NRAD 64 element core [1]. The specific simulation of interest is the bounding reactivity insertion accident (RIA) that includes the sudden insertion of a positive reactivity experiment as well as the sudden removal of all control rods. The magnitude of the reactivity insertion is approximately \$4.00 using a beta-effective of 0.0070 [2]. Special attention is given to the behavior of the peaking factors as a function of time since they are used in the safety analysis to determine the peak fuel temperature under adiabatic conditions.

Methodology

In this work, the continuous-energy Monte Carlo code Serpent version 2.1.27 [3] is employed to prepare cross sections for the MAMMOTH [4] deterministic model. MAMMOTH is a reactor physics application based on the MOOSE framework [5]. MAMMOTH uses the Rattlesnake [6] application to solve the neutron transport equation. A variety of solution schemes for the neutron transport equation are available including Point Reactor Kinetics and neutron diffusion, which are both used in this work. The neutron cross sections obtained from Serpent are corrected using the SPH procedure in MAMMOTH [7] in an attempt to preserved the Monte Carlo reaction rates in the various cross section zones. In addition, MAMMOTH is capable of computing dynamic reactivity as well as point reactor kinetic parameters as a function of time via adjoint weighting. The following versions were used in the transient calculations: MAMMOTH (12a42c6), Rattlesnake (8770c4f), YAK (b401c68), and BISON (derived from v1.2 ad3e9f4).

Cross Section Preparation with Serpent

Serpent was used to calculate a high fidelity steady state solution to the k-eigenvalue neutron transport problem. Along with the eigenvalue, homogeneous cross-sections were generated and used in subsequent transient analyses. All dimensions and material properties for the Serpent model were taken from the ICSBEP benchmark [8]. However, the NRAD benchmark model itself was modified in such a way as to allow proper cross-section generation in all spectral regions.

The Serpent model consists of 64 low-enriched UZrH fuel elements, 3 control rods, 1 water hole, 4 graphite reflector rods, and 12 graphite reflector blocks. The fuel elements, graphite rods, and control rods are grouped into 2x2 clusters with a constant pitch of 3.8862 cm. These clusters are then arranged, along with the peripheral graphite reflector blocks, into a 6x6 array. The x and y pitch between the clusters are equal to 4.05003 cm and 3.85445 cm, respectively. The core sits in a tank with a height and diameter of approximately 151 cm and 90 cm, respectively. The Serpent input also contains the 2 beam ports, shown in Figure 1. Both measure 13.97 cm wide and have a height equal to 16.51 cm. These regions are modeled as containing just air.

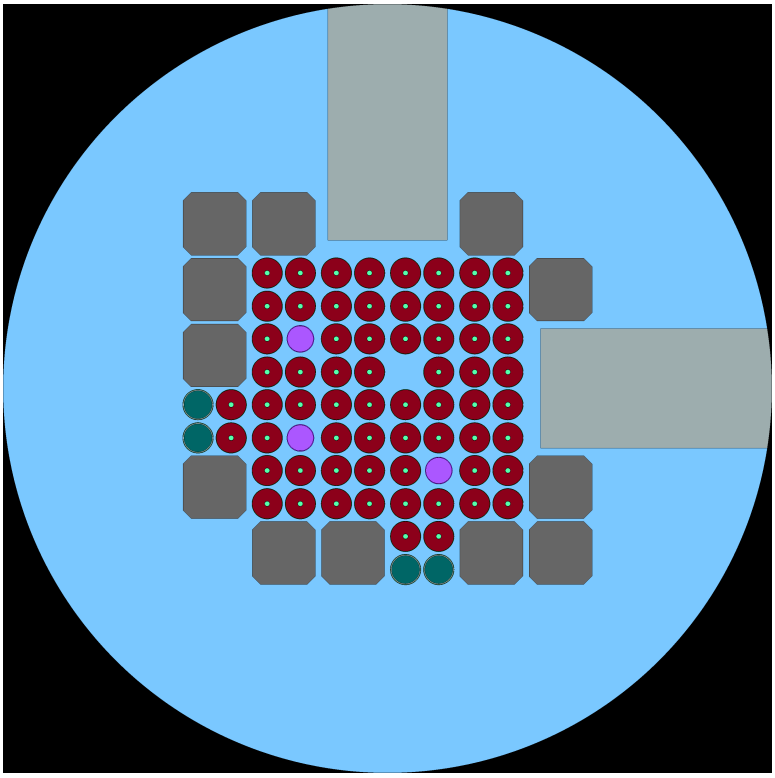

Figure 1. Serpent Model Showing Beam Port Detail

The cross section generation tasks seeks to separate regions with different materials (where possible) and regions with similar material but different neutron spectra. A number of independent radial spectral regions shown in Figure 2 were designated based on symmetry and physical location within the core, e.g. fuel regions with one side facing the reflector and all other sides facing fuel are assigned the same number. Each radial region contains 22 axial cross section regions. The following region numbering was used:

1. Regions 1100 – 3600 for fuel rods.
2. Regions 4100 – 4400 for the control rod and water regions.
3. Regions 5000 – 5800 for graphite reflector regions.
4. Regions 7200, 7400, 7500, 7700, and 9200 for the east beam port.
5. Regions 6200, 6400, 6500, 6700, and 9300 for the north beam port.
6. Regions 9000 and 9900 for the radial water reflector.

9900	9900	9900	9900	9900	9900	9503	9503	9503	9503	9900	9900	9900	9900	9900	9900
9900	9000	9000	9000	9000	9000	9300	9300	9300	9300	9000	9000	9000	9000	9000	9900
9900	9000	5000	5100	5100	5300	6400	6400	6700	6700	5300	5000	4300	9000	9000	9900
9900	9000	5100	5200	5400	5400	6200	6200	6500	6500	5500	5700	4400	4300	9000	9900
9900	9000	5100	5400	1100	1300	1400	1500	1500	1400	1300	1200	5700	5000	9000	9900
9900	9000	5100	5400	1600	1700	2300	2400	2400	2400	2400	1300	5500	5300	9000	9900
9900	9000	5100	5400	1900	4100	2000	2900	2500	2600	2400	1400	7700	7500	9200	9502
9900	9000	5600	5500	1600	1800	2300	3000	4200	2500	2400	1500	7700	7500	9200	9502
9900	9000	5800	3400	3300	1800	2300	2900	2800	2700	2400	1500	7200	7400	9200	9502
9900	9000	5800	3400	2200	4100	2000	2400	2300	1700	2300	1400	7200	7400	9200	9502
9900	9000	5600	5500	1600	1700	2300	2400	2100	4100	2000	1300	5500	5300	9000	9900
9900	9000	5000	5700	1200	3100	3100	3200	3300	1800	3600	1100	5400	5100	9000	9900
9900	9000	4300	4400	5700	5400	5400	5500	3500	3500	5500	5400	5200	5100	9000	9900
9900	9000	9000	4300	5000	5100	5100	5600	5800	5800	5600	5100	5100	5000	9000	9900
9900	9000	9000	9000	9000	9000	9000	9000	9000	9000	9000	9000	9000	9000	9000	9900
9900	9900	9900	9900	9900	9900	9900	9900	9900	9900	9900	9900	9900	9900	9900	9900

Figure 2. Radial Cross Section Regions for the NRAD 64 Core

The cross sections were based on ENDF/B-VII.r0 and were condensed to the 7 energy groups used in previous calculation by GA [1]. The cross sections were tabulated for the state points included in Table 1. Only the state points indicated with an "X" were calculated and included in the final tabulation. The control rod position was expressed as a translated distance from the reference fully inserted position. Therefore, CR0 is located 20.5875 cm above the bottom of the active core interface.

Table 1. State Points Used in the Functionalization of the Cross Sections

Fuel Temp [K]	CR0 (20.5875 cm)	CR1 (24.5875 cm)	CR2 (28.72867 cm)	CR3 (32.72867 cm)	CR4 (36.98368 cm)
313.15	X	X	X	X	X
473.15	X	X	X	X	X
553.15	X	X	X	X	X
673.15	X	X	X	X	X
973.15			X	X	X
1200.00			X	X	X

MAMMOTH Spatial Dynamics Analysis Model

The MAMMOTH model uses a cylindrical representation of the water reflector and explicitly models the beam ports as shown in the finite element mesh in Figure 3. The mesh contains both structured and unstructured grids with hexahedron elements in the former and wedge elements in the latter. Each fuel rod is represented by 16 elements in one X-Y plane and 16 axial planes. Therefore the axial discretization consists roughly of elements 2.5 cm in height. The movement of the control rods is introduced with a MOOSE function that linearly interpolates the location of the control rod as a function of time. The control rods are linearly withdrawn over the course of 0.5 sec. There could be some sensitivity in the manner the control rods are withdrawn from the core, which can be investigated in the future.

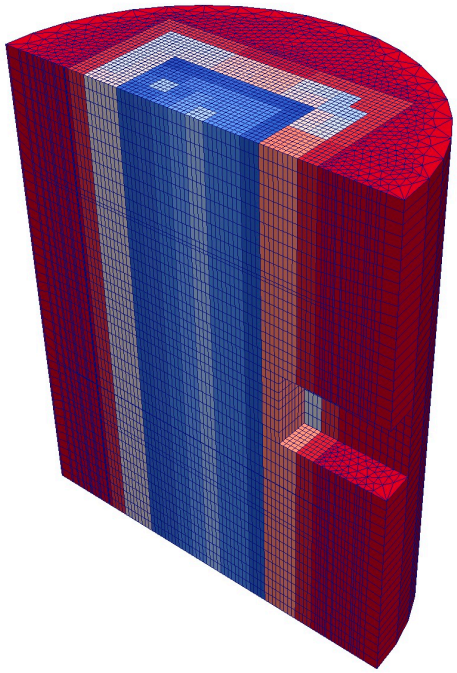

Figure 3. MAMMOTH Mesh for the NRAD 64 Element Core

Temperature coefficients of reactivity were calculated with MAMMOTH to ascertain the static feedback behavior of the model. The effective multiplication factors, reactivity changes and computed reactivity coefficients are included in Table 2. The results obtained compare well with GA values [2] and a plot of the reactivity versus temperature is shown in Figure 4 for both MAMMOTH and GA values. It is worth noting that the GA values are based on isothermal All Rods Out (ARO) conditions. The MAMMOTH calculations are based on an approximate ARO configuration (control rods at 1.12 centimeters from the fully withdrawn position) with an isothermal temperature of 313.15 K (40^{o}C) for the non-fuel materials in the core. The fuel temperature is the only parameter changed. The results indicate that the MAMMOTH model has slightly stronger feedback than that calculated by GA.

Table 2. Reactivity Change with Temperature, ARO

Fuel Temperature [K] (Other materials at 313.15 K)	$\mathbf{k_{eff}}$	$\Delta\rho = \frac{k_2 - k_1}{k_2 k_1}$	$\alpha_{2,1}$ [Δk/k-K]
313.15	1.02328		
473.15	1.01394	-9.21E-03	-5.76E-05
553.15	1.00799	-5.90E-03	-7.38E-05
673.15	0.99761	-1.04E-02	-8.67E-05
973.15	0.96484	-3.40E-02	-1.13E-04
1200.00	0.93685	-2.99E-02	-1.32E-04

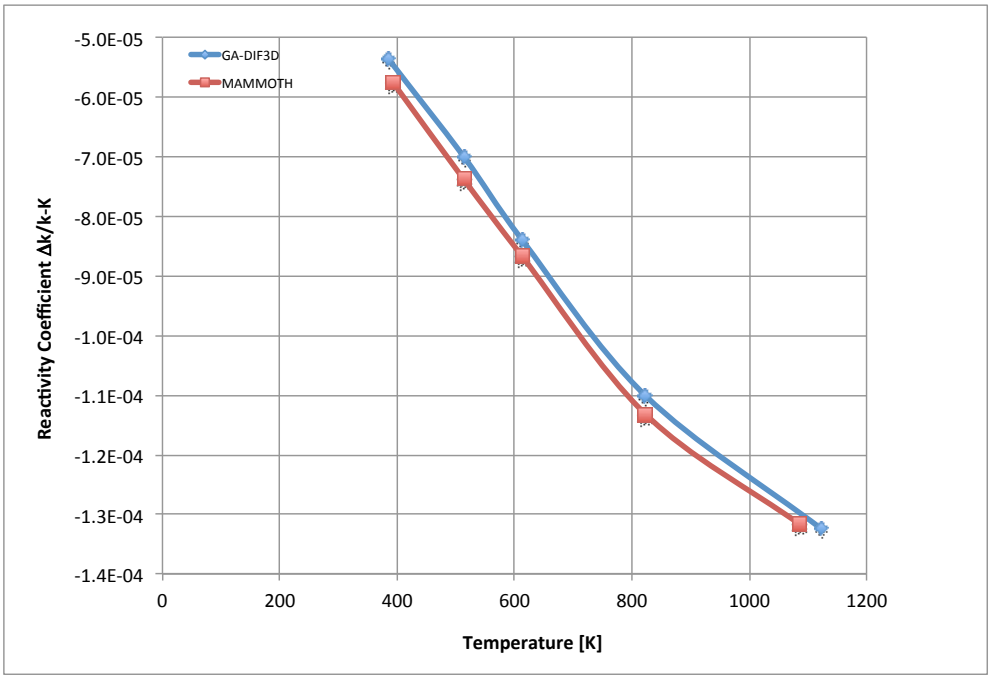

Figure 4. Temperature Coefficient of Reactivity

MAMMOTH Point Reactor Kinetics Analysis Model

In order to maintain some consistency between the PRK and the 3-D SD model, the reactor parameters were developed from the improved quasi-static method. The development of these parameters required the specification of an adjoint function used as a weighting function. Two adjoint state points at 313.15 K, one with CRs at the pre-transient position and one with CRs withdrawn, were used to determine the sensitivities of the parameters to the adjoint function and were found to have little effect. The variation of the effective delayed neutron fraction (β_{eff}) and the mean neutron generation time (Λ) was investigated, and β_{eff} was determined to have very little variation to warrant further consideration. The calculated value of the effective delayed neutron fraction was

$$\beta_{eff} = 0.007875.$$

On the other hand, the change in the Λ over time was significant enough to warrant using the two extrema of the distribution in two separate PRK calculations to determine the sensitivity to this parameter. The values of the mean neutron generation time were

$$\Lambda = 2.975\text{x}10^{-5} \; and \; 3.182\text{x}10^{-5} \; sec.$$

The PRK reactivity insertion model was based on the steady state points calculated at the isothermal temperature of 313.15K (40^{o}C) with the control rods at various positions as shown in Table 3. The total reactivity inserted is 0.02863, which assuming a beta of 0.007875 corresponds to \$3.63. If a β_{eff} = 0.007 is used instead, the reactivity insertion corresponds to \$4.09. It is important to emphasize that the PRK model is very sensitive to the reactivity insertion model. This reactivity insertion model is based on a single temperature it is unable to accurately capture the reactivity insertion in the core as it heats up. Conversely, the SD model provides a much better representation of the instantaneous reactivity of the core. Future sensitivity calculations should be conducted to properly bound the values produced by the PRK model, thus assuring the necessary level of conservatism is maintained.

Table 3. Reactivity Model for the PRK

SD model CR Position	**k_{eff}**	**$\Delta k/k$**
CR0	0.99480	
CR1	1.00448	0.00974
CR2	1.01283	0.01813
CR3	1.01915	0.02448
CR4	1.02328	0.02863

Since the purpose of this work is to compare similar PRK and SD models, the values of the six group βs and lambda calculated with the MAMMOTH SD model are used in the PRK model. This means that the actual static reactivity is less than \$4.

Thermal Analysis Model

The transient studies included in this report use a simple adiabatic model (no heat flow through the boundaries) for the fuel temperature field solution during the transient. The adiabatic model has the form:

$$\frac{\partial T(r,t)}{\partial t} = \epsilon \, \kappa(T(r),t)\Sigma_f(T(r),t)\psi(T(r),t)$$

where

$\psi(T(r),t)$ is the scalar flux [n/cm2-s]

$\Sigma_f(T(r),t)$ is the fission cross section [cm-1]

$\kappa(T(r),t)$ is the energy release per fission [J/fission]

$\epsilon = \frac{1}{\rho Cp}$

The density of fuel (2.14 g/cc) and the heat capacity are based on GA [9]. The specific heat capacity is functionalized with

$$C_p = 1.145206643 + 2.13808\text{x}10^{-3} * (t - 298.15) \qquad [J/g/K].$$

The fuel rods are homogenized (not modeled explicitly) in the MAMMOTH spatial model and the volume that represents a fuel rod is larger than the physical fuel volume. In order to obtain the correct energy deposition and the corresponding temperature increase, the fuel density is reduced appropriately in order to conserve the total mass of material within the mesh.

Results

The core power and temperature as a function of time are shown in Figures 5 and 6, respectively. The SD model predicts a peak power of 600.0 MW, whereas both PRK results are approximately at 855 MW. This discrepancy could be due to differences in the reactivity model, since small changes to the reactivity model in the PRK solution can lead to large changes in the peak power computed. The dynamic reactivity for all models is included in Figure 7. The lower reactivity of the spatial dynamics model yields both lower powers and temperatures.

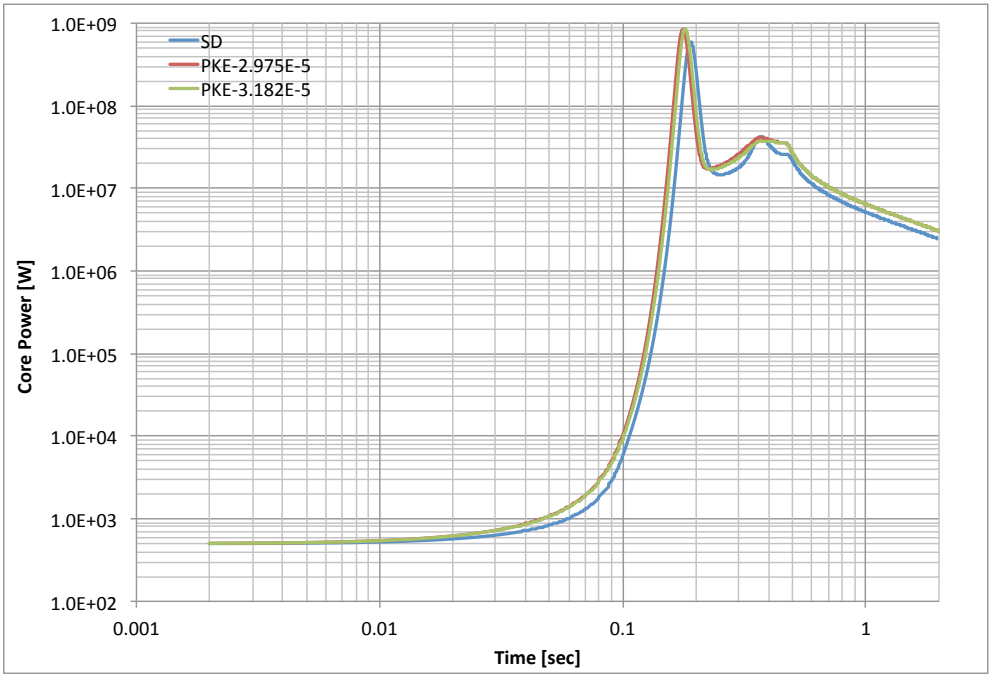

Figure 5. Power Transient Profile

The maximum fuel temperature reported is the maximum temperature in the mesh and is not the maximum temperature inside a fuel rod. To improve the calculation, detailed fuel models could be developed and readily coupled to the current spatial model.

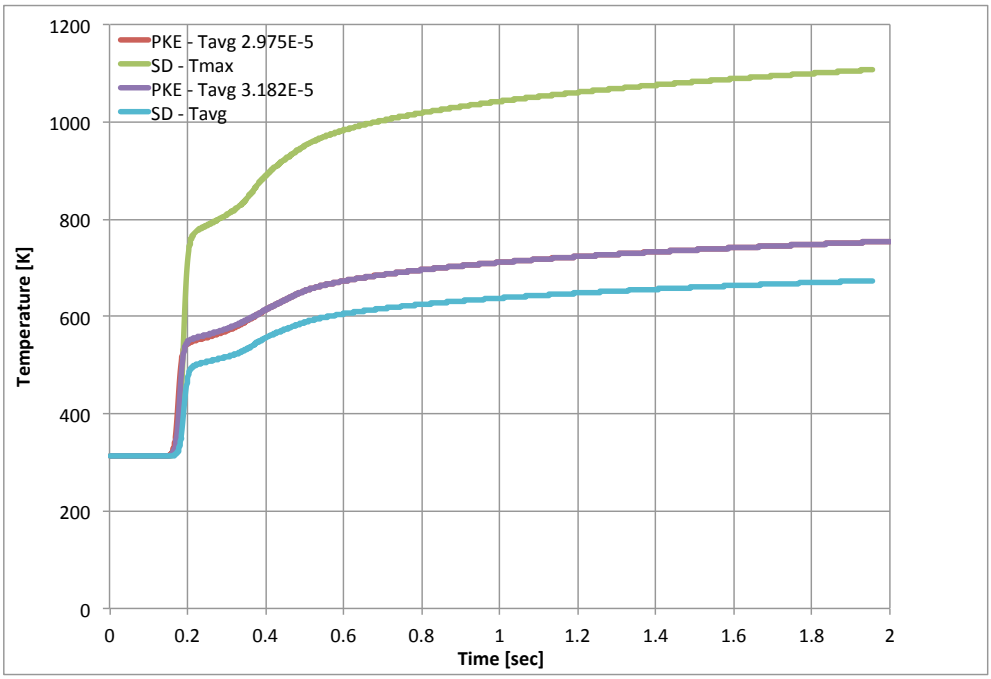

Figure 6. Fuel Temperature Profile

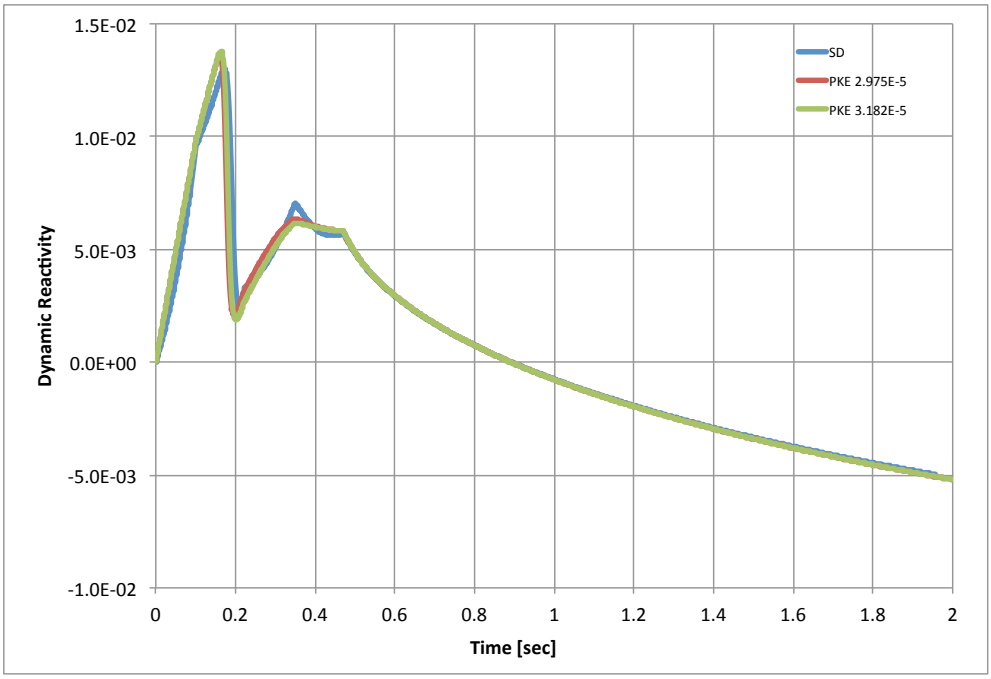

Figure 7. Dynamic Reactivity

Peaking factors at isothermal conditions with a core temperature of 313.15 K (40 ^{o}C), ARO are compared with GA calculations [2] in Table 4 and shown good consistency. Additionally, peaking factors for the SD simulation at the pre-transient configuration are shown in Table 5. Note that all of the peaking factors are higher in this configuration since the control rod position pushes the power towards the bottom of the core. The peaking factors obtained during the transient are reported in Table 6. The locations of the peaking factors provided in Tables 4 through 6 are based on the map shown in Figure 8. The Hot Rod Power Factor (HRPF) location is by the water hole before and during the transient. The Peak-to-Average Power Ratio starts (APR) by the west side of the control rod (APR1) and shifts to the south side of the same control rod during the transient (APR2). Finally, the Rod Peaking Factor (RPF) is located north of the control rod and approximately 3.87 cm above the interface at the bottom of the active core. In all cases the calculated transient peaking factors are below the steady state values at the pre-transient configuration. This is shown graphically in Figures 9 through 11.

Table 4. Peaking Factors at Steady State ARO

	GA ARO Table 2-5 [2]	**MAMMOTH 313.15 K**	**MAMMOTH Location**
Hot Rod Power Factor, $max\left\{\frac{\bar{P}_{rod}}{\bar{P}_{core}}\right\}$	1.585	1.557	(6,6)
Peak-to-Average Power Ratio, $max\left\{\frac{\hat{P}_{axial,rod}}{\bar{P}_{axial,rod}}\right\}$	1.290	1.237	(3,8)
Rod Peaking Factor, $max\left\{\frac{\hat{P}_{radial,rod}}{\bar{P}_{radial,rod}}\right\}$	1.600	1.606	(3,3,1)

Table 5. Peaking Factors at Steady State Pre-Transient Position

	MAMMOTH 313.15 K	**MAMMOTH Location**
Hot Rod Power Factor, $max\left\{\frac{\bar{P}_{rod}}{\bar{P}_{core}}\right\}$	1.675	(6,6)
Peak-to-Average Power Ratio, $max\left\{\frac{\hat{P}_{axial,rod}}{\bar{P}_{axial,rod}}\right\}$	1.550	(2,7)
Rod Peaking Factor, $max\left\{\frac{\hat{P}_{radial,rod}}{\bar{P}_{radial,rod}}\right\}$	1.617	(3,3,1)

Table 6. Peaking Factors During the Transient

	Transient maximum	**Transient Location**
Hot Rod Power Factor, $max\left\{\frac{\bar{P}_{rod}}{\bar{P}_{core}}\right\}$	1.675	(6,6)
Peak-to-Average Power Ratio, $max\left\{\frac{\hat{P}_{axial,rod}}{\bar{P}_{axial,rod}}\right\}$	1.550 / 1.390	(2,7) / (3,8)
Rod Peaking Factor, $max\left\{\frac{\hat{P}_{radial,rod}}{\bar{P}_{radial,rod}}\right\}$	1.617	(3,3,1)

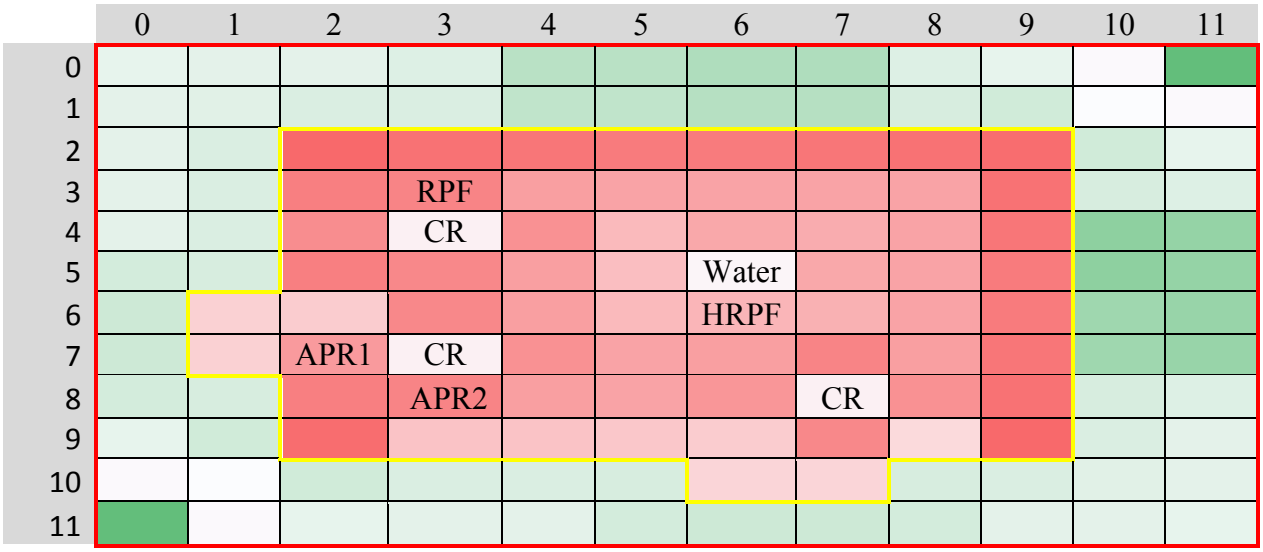

Figure 8. Location of the Peaking Factors

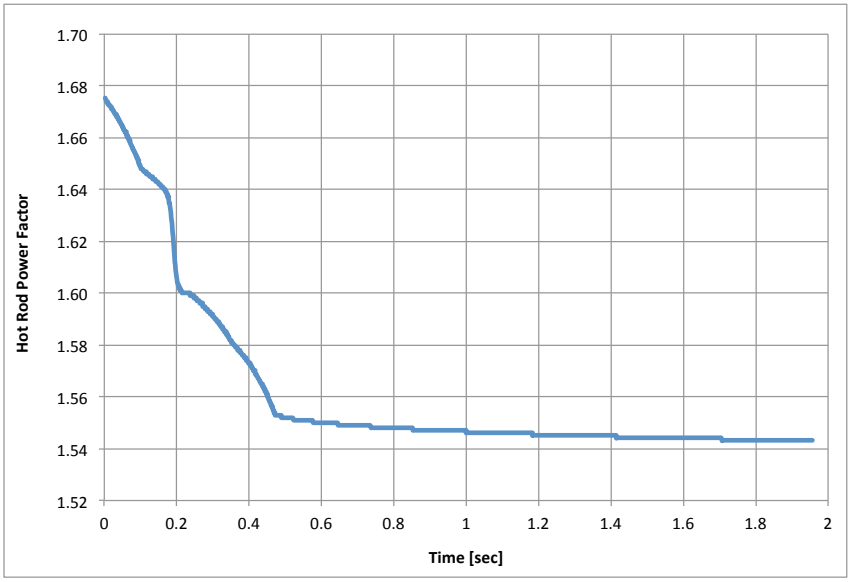

Figure 9. Maximum Value of the Hot Rod Power Factor as a Function of Time

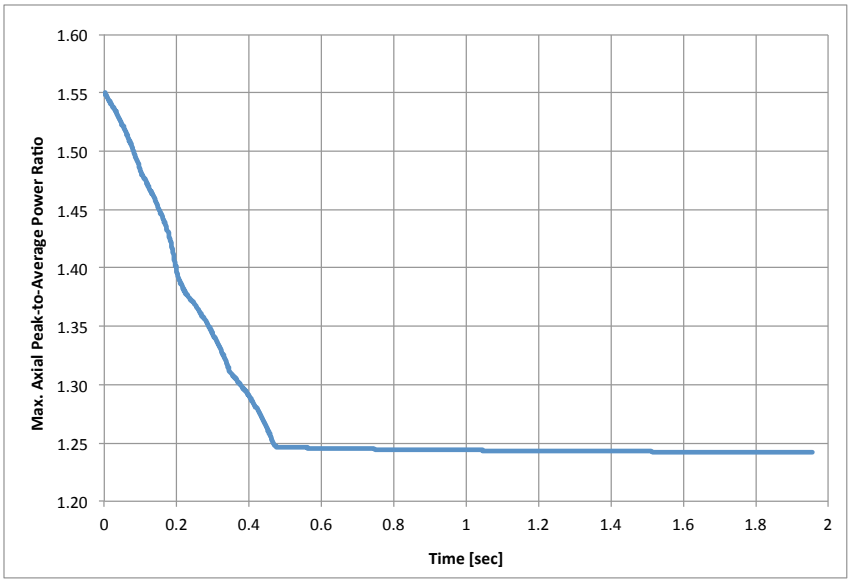

Figure 10. Maximum Value of the Axial Peaking Factor as a Function of Time

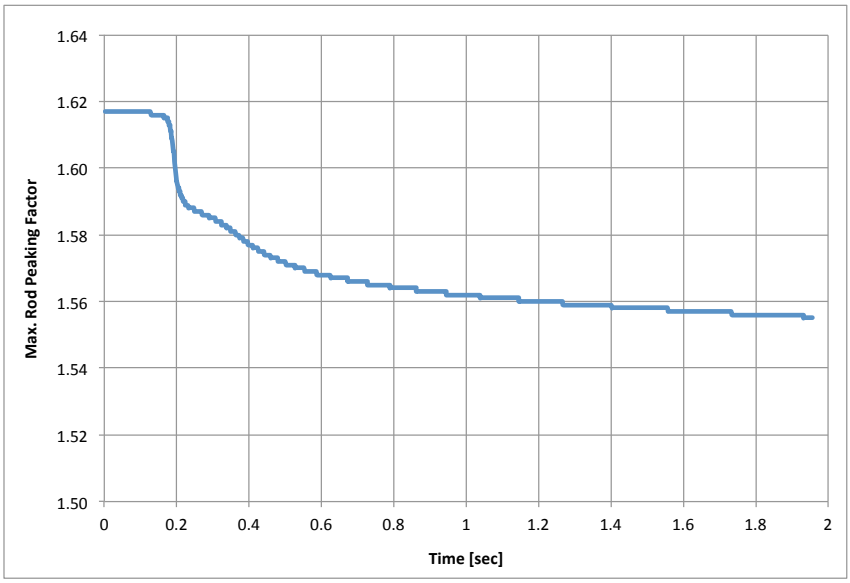

Figure 11. Maximum Value of the Local Peaking Factor as a Function of Time

Conclusions

This work shows that the MAMMOTH spatial model developed at the INL has consistent characteristics (reactivity coefficients and peaking factors) with the GA model used in previous studies [2]. The reactivity introduced in the transient is \$3.64, which is lower than \$4, but this is mainly due to the value of beta-effective calculated in the MAMMOTH model of (0.00787) versus that used in the GA calculation (0.007). The spatial dynamics simulation produces core powers and temperatures that are lower than the point kinetics counterpart. The PRK model displays a high sensitivity to the reactivity insertion model. The reactivity insertion model based on cold steady state conditions appears to be conservative compared to the spatial dynamics simulation, but further analyses are necessary to properly bound this conclusion. Finally, in all cases the calculated transient peaking factors are below the steady state pre-transient configuration values, but not below the values obtained in the ARO steady state configuration.

References

1. "LEU Upgrade of the NRAD Reactor Final Report," General Atomics 911193, August 2010.

2. "Impact of Beta Effective on Limiting Reactivity Accident," General Atomics Report 39296R00001, October 2011.

3. J. Leppänen. "Development of a New Monte Carlo Reactor Physics Code," Ph.D. Thesis, Helsinki University of Technology, Helsinki, Finland (2007).

4. F. N. Gleicher, et. al. "The Coupling of the Neutron Transport Application RATTLESNAKE to the Fuels Performance Application BISON," International Conference on Reactor Physics (PHYSOR 2014), Kyoto, Japan, (May 2014).

5. D. Gaston, C. Newman, G. Hansen, and D. Lebrun-Grand'e, "MOOSE: A parallel computational framework for coupled systems of non- linear equations," Nucl. Eng. Design, 239, pp. 1768-1778 (2009).

6. Y. WANG. "Nonlinear Diffusion Acceleration for the Multigroup Transport Equation Discretized with Sn and Continuous FEM With Rattlesnake," Proceedings to the International Conference on Mathematics, Computational Methods & Reactor Physics (M&C 2013), Sun Valley, Idaho, USA (May 2013).

7. A. Laurier, "Implementation of the SPH Procedure within the MOOSE Finite Element Framework," M.S. Thesis, École Polytechnique de Montréal, Montréal, Canada (2016).

8. John D. Bess, Thomas L. Maddock, Margaret A. Marshall, Leland M. Montierth, Ning Zhang, Ann Marie Phillips, Kenneth A. Schreck, J. Blair Briggs, Eric W. Woolstenhulme, John M. Bolin, Anthony Veca, Richard D. McKnight, Richard M. Lell, "Fresh-Core Reload of the Neutron Radiography (NRAD) Reactor with Uranium (20)-Erbium-Zirconium-Hydride Fuel," INL/EXT-10-19486, March 2014.

9. G.B. West et al. "Kinetic Behavior of TRIGA Reactors," General Atomics report GA-7882, March 1967.